Journal of Materials Science: Materials in Electronics (2018) 29:6548–6555
https://doi.org/10.1007/s10854-018-8638-7

Dy^{3+} Doped $Ca_9Gd(PO_4)_7$: a novel single-phase full-color emitting phosphor

Lurong Yang[1,2] · Zhongfei Mu[1] · Shaoan Zhang[3] · Qiang Wang[4] · Daoyun Zhu[1] · Yu Zhao[1] · Dongxiang Luo[4] · Qingtian Zhang[4] · Fugen Wu[4]

Received: 26 September 2017 / Accepted: 19 January 2018 / Published online: 23 January 2018

Abstract
A series of un-doped and Dy^{3+} doped $Ca_9Gd(PO_4)_7$ phosphors were synthesized by traditional solid state reactions. X-ray diffraction analysis and scanning electronic microscope observation were carried out to examine the phase formation and morphology of prepared samples. Emission spectra under the excitation at 350 nm ultraviolet light turn out that main emission bands are located at 480, 570 and 659 nm, which can be assigned to the optical transitions $^4F_{9/2} \rightarrow {}^6H_{15/2}$, $^4F_{9/2} \rightarrow {}^6H_{13/2}$ and $^4F_{9/2} \rightarrow {}^6H_{11/2}$ of Dy^{3+}, respectively. Comparison of emission spectra upon excitation of 273 nm between un-doped and Dy^{3+} doped $Ca_9Gd(PO_4)_7$ samples proves that effective energy transfer from Gd^{3+} to Dy^{3+} takes place. The Commission International de I'Eclairage color coordinates (0.272, 0.322) located in white region was achieved. With the increasing doping concentration of Dy^{3+}, concentration quenching is clearly observed and the optimum content of doped Dy^{3+} is 0.12. The mechanism of concentration quenching is experimentally ascertained to be electric dipole–dipole interactions. The study of quantum efficiency and thermal stability shows that our phosphors have higher quantum efficiency and better thermal stability. This work indicates that our phosphors have potential applications in white light-emitting diodes.

1 Introduction

Nowadays, white light-emitting diodes (wLEDs) have obtained extensive applications in lighting, display, plant growth regulation and in situ imaging of organisms because of their advantages of energy saving, environmental friendliness, high efficiency, long life, and so on [1–3]. Combination of a single LED chip with a single phosphor might be the simplest approach to obtain white light. Based on this point of view, the first method has been widely used, namely, combining a blue LED chip with a yellow phosphor (YAG: Ce^{3+}). White light obtained by this method has some vital drawbacks such as halo effect due to the different emission characteristics of the LEDs (directional) and the phosphors (isotropic), low color rendering index (CRI) and high color temperature caused by lack of red component in the spectra [4, 5]. The second method, that is, combining an ultraviolet (UV) LED chip with a full-color phosphor, is also being widely studied. At present, the market share of white light obtained by this method is obviously inferior to that by the first method. However, people are still investing a lot of energy in this area, hoping to get some full-color phosphors with excellent performing [6, 7].

Dy^{3+} doped inorganic compounds are a kind of full-color phosphors that can be excited by an UV LED chips. In the past several decades, numerous studies have proved their application value and development potential [8–10]. Dy^{3+} is of great importance among the rare earth ions because of its 4f–4f transitions which lead to blue, yellow and red emission. The luminescence lines are located in the regions of 470–500, 570–600, and 650–680 nm due to the optical

✉ Zhongfei Mu
muzhongfei@gdut.edu.cn

Fugen Wu
wufg@gdut.edu.cn

1 Experimental Teaching Department, Guangdong University of Technology, Waihuan Xi Road, No.100, Guangzhou 510006, People's Republic of China

2 School of Physics & Optoelectronic Engineering, Guangdong University of Technology, Waihuan Xi Road, No.100, Guangzhou 510006, People's Republic of China

3 Basic Courses Department, Guangzhou Maritime University, Hongshan Three Road, No. 101, Guangzhou 510725, People's Republic of China

4 School of Materials and Energy, Guangdong University of Technology, Waihuan Xi Road, No.100, Guangzhou 510006, People's Republic of China

transitions $^4F_{9/2} \rightarrow {}^6H_{15/2}$, $^4F_{9/2} \rightarrow {}^6H_{13/2}$ and $^4F_{9/2} \rightarrow {}^6H_{11/2}$ of Dy^{3+}, respectively. Besides, it is well known that the emission light is different in color. This depends on whether the Dy^{3+} ions are located at the high-symmetry sites with inversion centers or the low-symmetry without inversion centers [11, 12]. Additionally, gadolinium ion is a good constituent cation in host crystals which can be substituted by other rare earth ions. More importantly, Gd^{3+} can emit UV light at around 310 nm under the excitation at 275 nm [13]. Energy transfer from Gd^{3+} to Dy^{3+} might occur in a single phase. Recently, single-phase full-color emitting phosphors for wLEDs with a phosphate as host have obtained exclusive attention because of their high thermal stability and low preparation cost. Up to date, many research groups have paid many efforts to phosphors based on phosphates hosts, such as $Ca_9Lu(PO_4)_7$: Eu^{2+}, Mn^{2+} [14], $CaZr_4(PO_4)_6$: Dy^{3+} [15], $Na_3Bi(PO_4)_2$: Tb^{3+}, Sm^{3+} [16] and $Sr_3Y(PO_4)_3$: Dy^{3+} [17], etc.

Herein, we present Dy^{3+} doped $Ca_9Gd(PO_4)_7$ phosphors synthesized through solid state reactions. The structure, morphology, luminescence properties and energy transfer from Gd^{3+} to Dy^{3+} were investigated in detail. The application of these phosphors for wLEDs has also been referred.

2 Experimental

2.1 Sample preparation

The$Ca_9Gd_{1-x}(PO_4)_7$: xDy^{3+} ($x = 0$, 0.02, 0.04, 0.06, 0.08, 0.10, 0.12, 0.14, 0.16, 0.18) phosphors were synthesized via conventional high temperature solid state reactions. High purity powders of $CaCO_3$ (99%), Gd_2O_3 (99.99%), $(NH_4)H_2PO_4$ (99%) and Dy_2O_3 (99.99%) were weighed according to a certain stoichiometric ratio as starting materials. Then, the weighed powders were mixed thoroughly in an agate mortar. Subsequently, the mixtures were placed in alumina crucibles followed by calcination in a tubular furnace at 1200 °C for 6 h in air. Finally, the samples were cooled down to room temperature (RM) naturally and ground into powder for characterization.

2.2 Sample characterization

The phase purity of as-prepared samples were employed by a PGENERAL XD-2 powder X-ray diffractometer with Cu-Kα irradiation ($\lambda = 1.5406$ Å) under 36 kV tube voltage and 20 mA tube current in 2θ ranging from 10° to 70°.The morphology of the samples was evaluated by a Hitachi S-3400N scanning electronic microscope (SEM) under 15 kV accelerating voltage. The photoluminescence (PL) and photoluminescence excitation (PLE) spectra were recorded using a Hitachi F-7000 fluorescence spectrophotometer equipped with a 150W Xe light source under 400V working voltage. The luminescence decay times were measured by an Edinburgh Instruments FLS-980 fluorescence spectrophotometer equipped with a 450 W Xenon lamp as the excitation source under 400 V working voltage. Diffuse reflectance spectra (DRS) were carried out with a Shimadzu UV-2450 UV–VIS-NIR spectrophotometer. Quantum efficiency and temperature-dependent PL spectra from room temperature to 300 °C were measured by another fluorescence spectrometer (Jobin Yvon Triax 320) equipped with double excitation mono-chromators and a homemade high temperature sample heater. Except for temperature-dependent PL spectra, all the measurements were carried out at RM.

3 Results and discussion

3.1 Phase purity

Figure 1 shows the X-ray diffraction (XRD) patterns of $Ca_9Gd_{1-x}(PO_4)_7$: xDy^{3+} phosphors with varied doping concentration of $Dy^{3+}(x)$. All the diffraction peaks of $Ca_9Gd_{1-x}(PO_4)_7$: xDy^{3+} phosphors can be indexed to the standard power diffraction card of $Ca_9Y(PO_4)_7$ (JCPDS No. 46-0402). No other secondary impurity phase is detected. This indicates that $Ca_9Gd(PO_4)_7$ has the same crystal structure as the $Ca_9Y(PO_4)_7$. The doping of Dy^{3+} with a small doping concentration does not change the crystal structure of $Ca_9Gd(PO_4)_7$. The effective radii of involved cations were reported as follows: R (Ca^{2+}) = 100 pm, R (Gd^{3+}) = 93.8 pm, R (Dy^{3+}) = 91. 2 pm, R (P^{5+}) = 17 pm [18]. On the basis of their identical charge and similar ionic radii, Dy^{3+} most probably occupies Gd^{3+} sites.

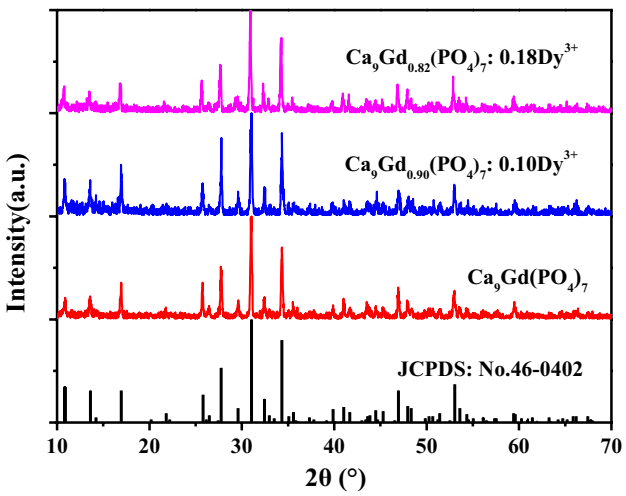

Fig. 1 XRD patterns of samples $Ca_9Gd_{1-x}(PO_4)_7$: xDy^{3+} ($x = 0$, 0.10, 0.18), the standard pattern of JCPDS card No. 46–0402 is also listed for comparison

3.2 Morphology observation

In order to observe the surface morphology of the synthesized phosphors, SEM observation was carried out. The typical SEM images are shown in Fig. 2. It is obviously observed that the samples consist of aggregated particles with a particle size ranging from 1 to 3 μm.

3.3 DRS research

Figure 3 depicts the DRS of un-doped $Ca_9Gd(PO_4)_7$ and a representative sample $Ca_9Gd_{0.88}(PO_4)_7$: $0.12Dy^{3+}$. It shows a noticeable absorption edge at about 320 nm. Before 320 nm, there are two absorption bands peaking at 273 and 214 nm. The former can be attributed to the $^8S_{7/2} \rightarrow {}^6I_J$ transition of Gd^{3+} ions whereas the latter might be related to the transition of the other cation in the host.

The band gaps of the un-doped and Dy^{3+} doped phosphors were calculated according to the DRS. The ratio of the light scattered from a thick layer of sample and ideal non-absorbing reference sample is measured as a function of the wavelength λ, $R_\infty = R_{sample}/R_{reference}$. In the diffuse reflectance spectra, the relation between absorption and scattering can be described via Kubelka–Munk Equation [19, 20]:

$$F(R_\infty) = \frac{(1-R_\infty)^2}{2R_\infty} = \frac{K}{S} \quad (1)$$

where R_∞ is the diffuse reflectance of the sample, K is absorption coefficient and S is scattering coefficient.

Furthermore, on the basis of Tauc relation, the band gap E_g and linear absorption coefficient α of a material can be expressed as follows:

$$\alpha h\nu = C_1(h\nu - E_g)^{\frac{n}{2}} \quad (2)$$

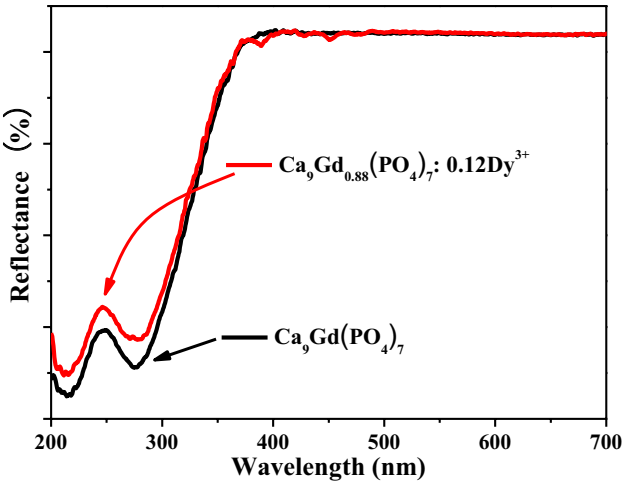

Fig. 3 DRS of $Ca_9Gd(PO_4)_7$ and $Ca_9Gd_{0.88}(PO_4)_7$: $0.12Dy^{3+}$

where hν and $C_1$is the photon energy and proportionality constant, respectively.

When the material scatters in perfectly diffuse manner (or when it is illuminated at 60 °C incidence), the absorption coefficient K becomes equal to 2α. Concerning that the scattering coefficient S as constant with respect to wavelength, and using Eqs. (1) and (2), it can be derived that:

$$[F(R_\infty)h\nu]^2 = C_2(h\nu - E_g)^n \quad (3)$$

The value of n is equal to 1, 2, 3, 4 and 6 for direct allowed transitions, non-metallic materials, direct forbidden transitions, indirect allowed transition and indirect forbidden transitions, respectively. Now, among the plot of $[F(R_\infty)\ h\nu]^2$, $[F(R_\infty)\ h\nu]$, $[F(R_\infty)\ h\nu]^{2/3}$, $[F(R_\infty)\ h\nu]^{1/2}$, $[F(R_\infty)\ h\nu]^{1/3}$ versus a function of photon energy hν, the best fitting was obtained when n = 1 in Eq. (3), which indicating that the band transitions took place are direct

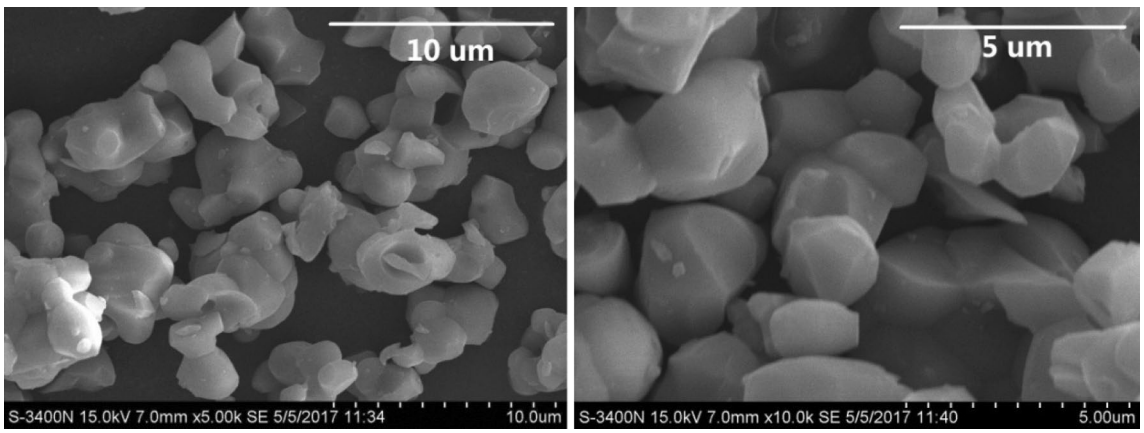

Fig. 2 SEM images of a representative sample $Ca_9Gd_{0.88}(PO_4)_7$: $0.12Dy^{3+}$ phosphor

in nature. Therefore, the band gaps of $Ca_9Gd(PO_4)_7$ and $Ca_9Gd_{0.88}(PO_4)_7$: $0.12Dy^{3+}$ were ascertained to be 3.88 and 3.87 eV by extrapolating the lines to $[F(R_\infty)\ h\nu]^2=0$, according to the plot of $[F(R_\infty)\ h\nu]^2$ versus $h\nu$, as shown in Fig. 4 (a) and (b).These values are similar to that of compounds with similar structure such as $Ca_8MgBi(PO_4)_7$(3.27 eV) [21], $Sr_9Sc(PO_4)_7$(3.92 eV) [22], $Ca_9La(PO_4)_7$ (3.96 eV) [23], $Ca_{10}Na(PO_4)_7$(4.1 eV) [24], and $Ca_9Bi(PO_4)_7$(4.25 eV) [25].

The top of the valence band of these compounds is mostly formed by O 2p and P3s, 3p states [26]. However, the bottom of conduction band is related with the other cation except for phosphorus ions. Thus the variation of band gap energy around 4 eV is mainly related to cation except for phosphorus ions. In this case, Ca^{2+} and Gd^{3+} are involved, which is embodied in the DRS. It is worth noting that the doping of luminescent centers can also change the band gap energy more or less. Zhang et al. found that the doping of Eu^{3+} with a content of 70% can increase the band gap energy of $Ca_8MgBi(PO_4)_7$ from 3.27 to 3.38 eV [21]. Our recent investigation also shows that the doping of Eu^{3+} with a big concentration can increase the band gap of $Ca_9La(PO_4)_7$ [23]. However, in this work, the band gap of $Ca_9Gd_{0.88}(PO_4)_7$: $0.12Dy^{3+}$ is slightly smaller than that of $Ca_9Gd(PO_4)_7$. There might be two reasons for this difference. On the one hand, Eu^{3+} in inorganic compounds can form $O^{2-}\rightarrow Eu^{3+}$ charge transfer band in the PLE spectra. This can remarkably change the band structure of inorganic compounds. However, there are only some sharp excitation peaks in the PLE spectra of Dy^{3+} doped phosphors. On the other hand, the doping concentration of Eu^{3+} is often much bigger than that of Dy^{3+}, even as high as 100%. Further research is needed to obtain deeper reasons.

3.4 Luminescence properties

The photoluminescence excitation (PLE) spectra with different doping concentration of Dy^{3+} monitoring the emission at 570 nm are displayed in Fig. 5. It is apparent that the PLE spectra comprises two parts: the first part from 250 to 320 nm contains tow peaks centered at 273 and 293 nm, corresponding to the $^8S_{7/2}\rightarrow{}^6I_{7/2}$ and $^8S_{7/2}\rightarrow{}^6P_{7/2}$ transitions of Gd^{3+} in the host [27, 28], respectively; and the other part from 300 to 460 nm consists of several bands located at 310, 323, 337, 350, 362, 386, 425 and 451 nm, which respectively results from $^6H_{15/2}\rightarrow{}^4D_{7/2}$, $^6H_{15/2}\rightarrow{}^6P_{3/2}$, $^6H_{15/2}\rightarrow{}^4F_{5/2}$, $^6H_{15/2}\rightarrow{}^6P_{7/2}$, $^6H_{15/2}\rightarrow{}^6P_{5/2}$, $^6H_{15/2}\rightarrow{}^6M_{21/2}$, $^6H_{15/2}\rightarrow{}^4G_{11/2}$ and $^6H_{15/2}\rightarrow{}^4I_{15/2}$ in the $4f^9$ electronic configurations of the

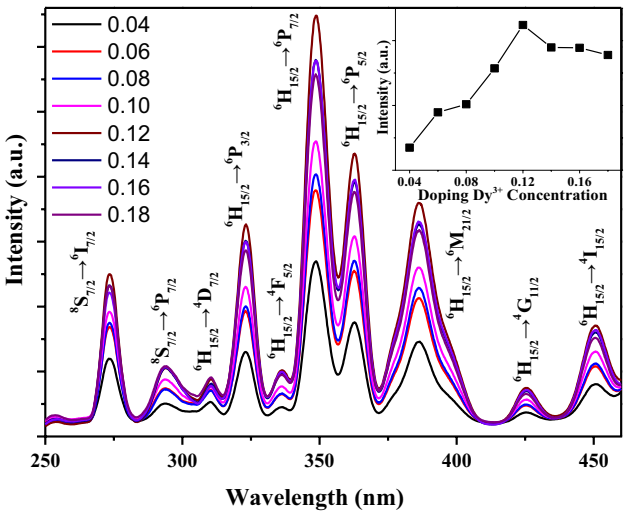

Fig. 5 PLE spectra of samples with different doping concentration of Dy^{3+} monitoring the emission at 570 nm (The inset shows the relationship of excitation intensity and doping concentration of Dy^{3+})

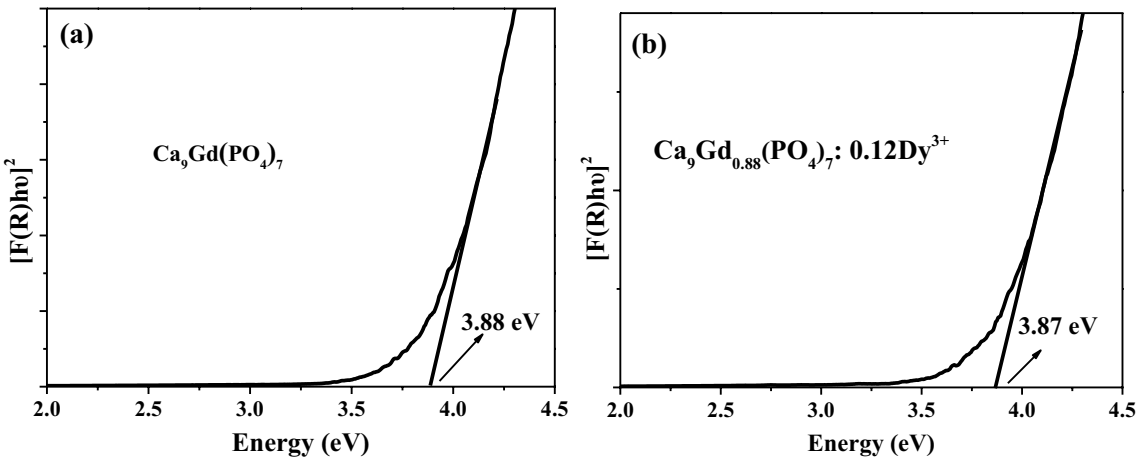

Fig. 4 Band gap values of $Ca_9Gd(PO_4)_7$ (**a**) and $Ca_9Gd_{0.88}(PO_4)_7$: $0.12Dy^{3+}$ (**b**)

Dy^{3+} ions [17]. The appearance of excitation peaks corresponding to Gd^{3+} in the PLE spectrum of Dy^{3+} doped samples indicates the occurrence of energy transfer from Gd^{3+} to Dy^{3+}.

As illustrated in Fig. 6, the photoluminescence (PL) spectra of Dy^{3+} of samples excited at 350 nm mainly consist of three emission peaks at 480, 570 and 659 nm, which can be assigned to the optical transitions $^4F_{9/2} \rightarrow {}^6H_{15/2}$, $^4F_{9/2} \rightarrow {}^6H_{13/2}$ and $^4F_{9/2} \rightarrow {}^6H_{11/2}$ of Dy^{3+}, respectively. The inset of Fig. 6 shows the relationship between the relative intensity of $^4F_{9/2} \rightarrow {}^6H_{15/2}$ transition and the doping concentration of Dy^{3+}. As the concentration increases, the emission intensity increases and reaches the maximum value at $x = 0.12$, which is taken as the optimum concentration. Beyond this optimum concentration, the intensity decreases due to the well-known concentration quenching effect.

In addition, it is generally accepted that when Dy^{3+} are located at high-symmetry sites with inversion centers, $^4F_{9/2} \rightarrow {}^6H_{15/2}$ magnetic dipole transition (blue emission) is dominant while $^4F_{9/2} \rightarrow {}^6H_{13/2}$ electric dipole transition (yellow emission) is prominent as Dy^{3+} ions are located at low-symmetry sites without inversion centers. In our experiment, the intensity at 480 nm is stronger than that at 570 nm for each samples, as displayed in Fig. 6, certifying that Dy^{3+} ions tend to occupy high-symmetry sites in the host.

3.5 Concentration effect

The concentration quenching phenomenon can be ascribed to non-radiative transition process between the activators and it can be represented by the critical distance R_c, the shortest average distance between the nearest activator Dy^{3+} ions at a critical concentration x_c.

Hence, the critical transfer distance (R_c) was described by Eq. (4) according to Blasse [29, 30].

$$R_c \approx 2\left(\frac{3V}{4\pi x_c N}\right)^{\frac{1}{3}} \tag{4}$$

Here x_c is the critical concentration from Fig. 6, N is the number of available sites in the unit cell which can be occupied by Dy^{3+} ions, and V is the volume of the unit cell. In this case, $x_c = 0.12$, $N = 6$ and $V = 3525.89\ Å^3$. Then, the value of R_c is calculated to be ~21.07 Å.

There are several mechanisms responsible for energy transfer, that is, radiation re-absorption, exchange interaction and multi-polar interaction [31, 32]. Radiation re-absorption needs an overlap between PLE spectrum of activators and PL spectrum of sensitizers. In this case, both activator and sensitizer are Dy^{3+}. There is no spectral overlap between PLE spectrum of activators and PL spectrum of sensitizers. Thus, radiation re-absorption is not accountable for the energy transfer among Dy^{3+}. Exchange interaction is usually accountable when the critical distance is smaller than 5 Å. The critical distance in this case is 21.07 Å which is much larger than 5 Å. In consequence, multi-polar interaction is the most important mechanism for energy transfer among Dy^{3+}. Concentration quenching mainly takes place due to electric multi-polar interaction among Dy^{3+}.

The type of the multi-polar interaction can be determined by the following Eq. (5) [32]:

$$\frac{I}{x} = K\left[1 + \beta(x)^{\frac{Q}{3}}\right]^{-1} \tag{5}$$

Here I is the emission intensity at activator concentration x, K and β are the constants under the same excitation condition in a specific host lattice. The values of $Q = 6, 8, 10$ correspond to dipole–dipole (d–d), dipole–quadrupole (d–q) and quadrupole–quadrupole (q–q) interactions, respectively. According to Eq. (5), the curve of log(I/x) vs. log(x) for the $^4F_{9/2} \rightarrow {}^6H_{15/2}$ transitions of Dy^{3+} ions in $Ca_9Gd_{1-x}(PO_4)_7$: xDy^{3+} is shown in Fig. 7. The fitting result in the region of high concentrations appears to be linear with a slope $(-Q/3) = 1.62$ which is approximately 2. The calculated value Q is approximately 6,which manifests that the d–d interaction is dominant for Dy^{3+} emission quenching mechanism in $Ca_9Gd(PO_4)_7$ host.

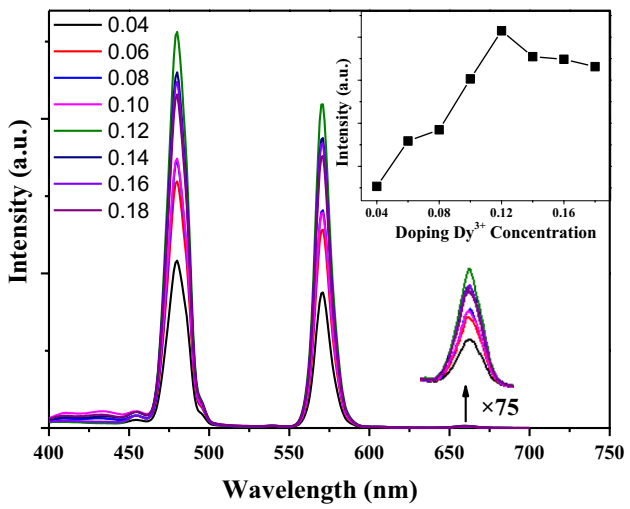

Fig. 6 PL spectra of samples with different doping concentration of Dy^{3+} excited with 350 nm (The inset shows the relationship of emission intensity and doping concentration of Dy^{3+})

3.6 Decay times

The luminescence decay curves of $Ca_9Gd_{1-x}(PO_4)_7$: xDy^{3+} phosphors recorded for the wavelength of 480 nm ($^4F_{9/2} \rightarrow {}^6H_{15/2}$)are presented in Fig. 8. Evidently, the curves

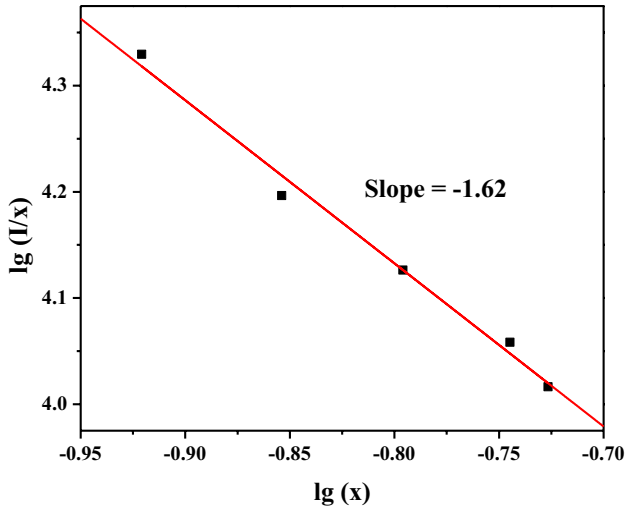

Fig. 7 The relationship of the concentration of Dy^{3+} ions log(x) and the log(I/x) for the $^4F_{9/2} \rightarrow {}^6H_{15/2}$ transitions

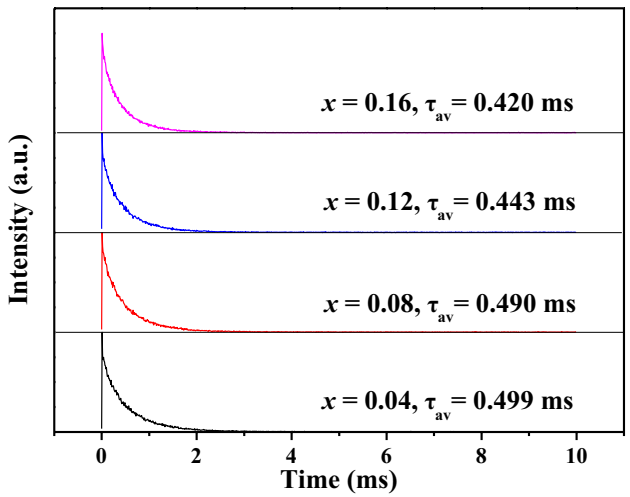

Fig. 8 Luminescence decay curves of $Ca_9Gd_{1-x}(PO_4)_7$: xDy^{3+} ($x = 0.04$, 0.08, 0.12, 0.16) phosphors excited at 350 nm and monitored at 480 nm

are successfully fitted by bi-exponential equation as follows [33]:

$$I = A_1 e^{-t/\tau_1} + A_2 e^{-t/\tau_2} \quad (6)$$

where I is the luminescence intensity; τ_1 and τ_2 are decay times for the exponential components; t is the time after excitation.

The average decay time τ_{av} can be calculated with the following equation:

$$\tau_{av} = \frac{A_1\tau_1^2 + A_2\tau_2^2}{A_1\tau_1 + A_2\tau_2} \quad (7)$$

The calculated average decay time τ_{av} are 0.499, 0.490, 0.443 and 0.420 ms, corresponding to $x = 0.04$, 0.08, 0.12 and 0.16, respectively. It is conspicuous that as the doping concentration of Dy^{3+}increases, the lifetime decreases gradually, which is put down to the decreasing average distance between the Dy^{3+} ions bring about the energy transfer between the Dy^{3+} ions. Owing to the energy transfer, the decay time decreases with the increasing rate of the non-radiative and self-absorption.

3.7 CIE chromaticity coordinates

The ratio of yellow to blue (Y/B) integrated emission intensity is usually used to estimate the distortion around Dy^{3+} ions [34, 35]. Also, the line linking the blue and yellow wavelength usually passes through the white light region according to the CIE 1931 chromaticity diagram, thus, the Y/B ratio is worth investigating. The calculated Y/B value for each sample is stable between 0.79 and 0.84, which strongly demonstrates that Dy^{3+} occupy high-symmetry sites in the host and the concentration of Dy^{3+} has little influence on the $Ca_9Gd(PO_4)_7$ crystal structure.

To further represent the color emission of the phosphors, a Commission International de I'Eclairage (CIE) plot is plotted in Fig. 9. The chromaticity coordinates of each sample with varied Dy^{3+} doping concentration were calculated from the PL spectra under 350 nm excitation. They were located at white region at approximate (0.272, 0.322) for Dy^{3+} doped phosphors.

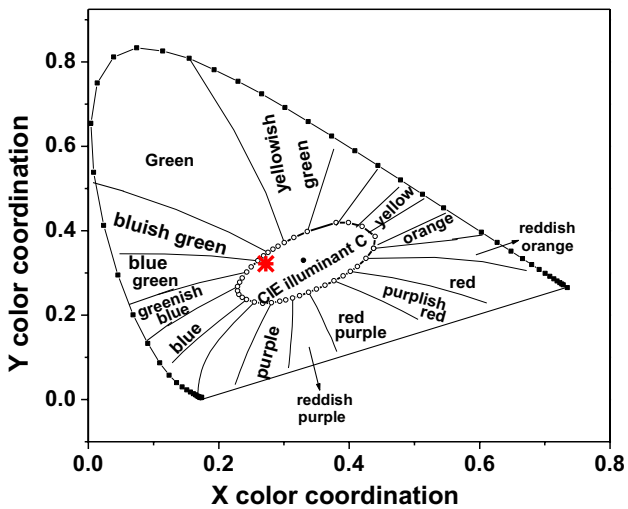

Fig. 9 CIE plot of $Ca_9Gd_{1-x}(PO_4)_7$: xDy^{3+} phosphors

3.8 Energy transfer from Gd^{3+} to Dy^{3+}

As mentioned above, the $^8S_{7/2} \rightarrow {}^6I_{7/2}$ and $^8S_{7/2} \rightarrow {}^6P_{7/2}$ transitions of Gd^{3+} ions in the host are clearly shown in the PLE spectra. Hence, energy transfer from Gd^{3+} to Dy^{3+} may occur in the $Ca_9Gd_{1-x}(PO_4)_7$: xDy^{3+} phosphor. To further investigate the energy transfer process, the PLE and PL spectra of un-doped $Ca_9Gd(PO_4)_7$ are shown in Fig. 10a and b. The sharp line at 273 nm originates from the $^8S_{7/2} \rightarrow {}^6I_{7/2}$ transition of Gd^{3+} ions, whereas the intensity emission line at 310 nm is ascribed to the $^6P_{7/2} \rightarrow {}^8S_{7/2}$ transitions. Meanwhile, the PL spectra of $Ca_9Gd_{0.88}(PO_4)_7$: $0.12Dy^{3+}$ pumped with 273 nm ultraviolet were measured, which is similar to the PL spectra pumped with 350 nm, consisting of two strong bands and a much weaker band, as depicted in Fig. 10d. The PLE spectra of $Ca_9Gd_{0.88}(PO_4)_7$: $0.12Dy^{3+}$ are also displayed in Fig. 10c. Furthermore, the strong sharp peak located at 310 nm can be detected, which stems from $^8S_{7/2} \rightarrow {}^6I_{7/2}$ transition of Gd^{3+} ions. The phenomenon clearly certifies that energy transfer from Gd^{3+} to Dy^{3+} does take place.

As vividly displayed in Fig. 11, energy level diagram shows the energy transfer process from Gd^{3+} to Dy^{3+}in $Ca_9Gd_{1-x}(PO_4)_7$: xDy^{3+}. Under the excitation of 273 nm UV light, electrons of Gd^{3+} in $Ca_9Gd_{1-x}(PO_4)_7$: xDy^{3+} are excited to the excited state of ^6I from the ground state of $^8S_{7/2}$ of Gd^{3+}. Afterwards, the energy is transferred to the $^6P_{3/2}$ level of Dy^{3+}. Subsequently, there is a non-radiative transition process among the excited states which resulted in transfer of electrons to the level of $^4F_{9/2}$. Ultimately, electrons return to ground states of Dy^{3+} and thereby give the characteristic emission [36, 37].

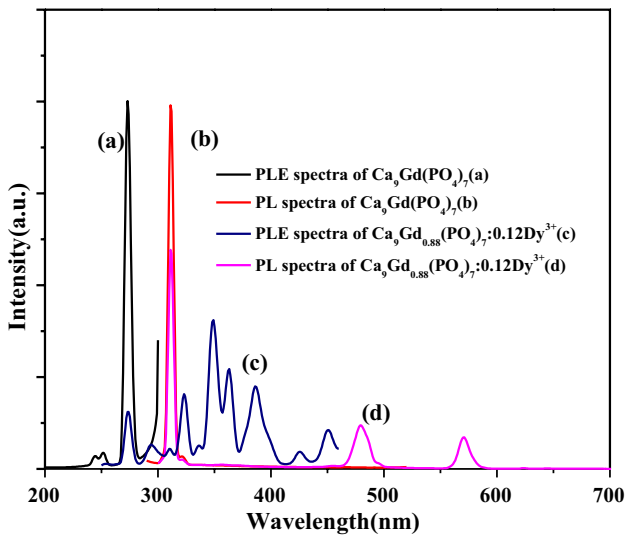

Fig. 10 PLE (**a**) and PL (**b**) spectra of un-doped $Ca_9Gd(PO_4)_7$, PLE (**c**) and PL (**d**) spectra of $Ca_9Gd_{0.88}(PO_4)_7$: $0.12Dy^{3+}$

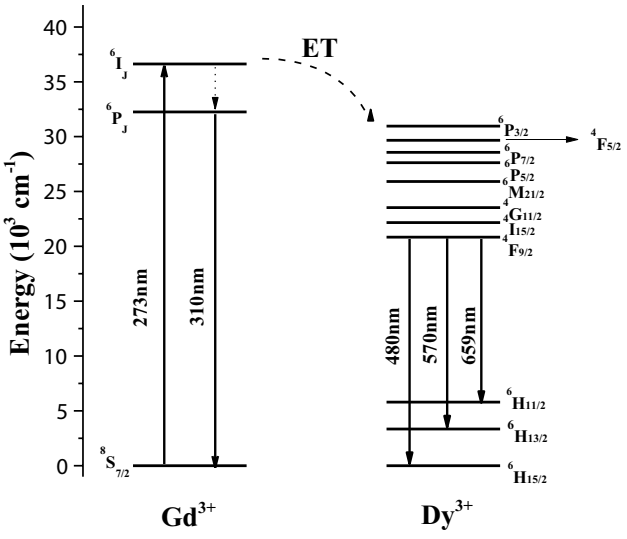

Fig. 11 Energy level diagram showing the energy transfer process from Gd^{3+} to Dy^{3+}

3.9 Quantum efficiency and thermal stability

Quantum efficiency and thermal stability of phosphors are two essential indexes to present the luminescence performance and to evaluate the suitability for the solid-state lighting applications. The internal quantum efficiency and external quantum efficiency of $Ca_9Gd_{0.88}(PO_4)_7$: $0.12Dy^{3+}$ are experimentally determined to be 19.9 and 9.2% under 350 nm excitation, respectively. Although these values do not seem to be high, considering that our preparation conditions are not optimal, these values have a room for further improvement.

Temperature-dependent PL spectra from 25 to 300 °C of a typical sample $Ca_9Gd_{0.88}(PO_4)_7$: $0.12Dy^{3+}$ are measured. With the increment of the temperature, the integral PL intensity decreases gradually. The relationship of the integral PL intensity of one representative sample $Ca_9Gd_{0.88}(PO_4)_7$: $0.12Dy^{3+}$ with temperature is shown in Fig. 12. With the increment of the temperature, the PL intensity decreases gradually for the well-known temperature quenching. The PL intensity at 100, 150 and 200 °C is about 85, 76, and 59% of the one at room temperature (25 °C), respectively. This indicates that our phosphors present a better thermal stability.

4 Conclusions

In summary, a series of white light emitting phosphors $Ca_9Gd(PO_4)_7$: Dy^{3+} were successfully prepared through solid state reactions. Obtained phosphors show strong emissions at around 480 and 570 nm as well as a feeble emission

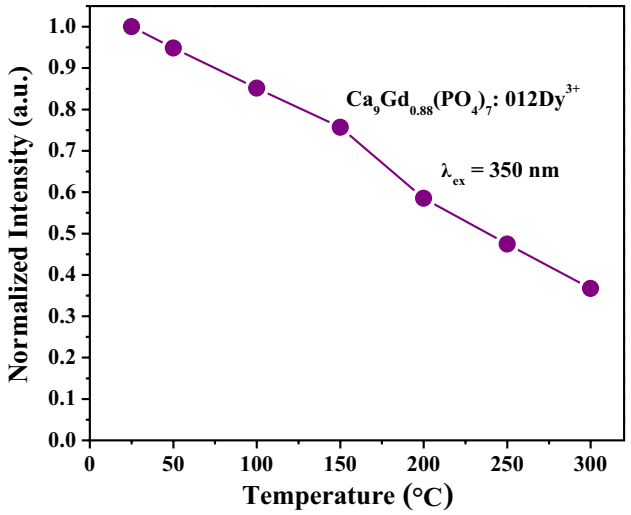

Fig. 12 Relationship of the integral PL intensity of one representative sample $Ca_9Gd_{0.88}(PO_4)_7$: $0.12Dy^{3+}$ with temperature

peak at 659 nm upon excitation with 350 nm UV light. Blue emission is prominent. This indicates that Dy^{3+} ions are located at high-symmetry sites with inversion centers. The optimum doping concentration of Dy^{3+} is experimentally determined to be 12 mol%. The concentration quenching mechanism is ascertained to be electric dipole–dipole interaction between Dy^{3+} ions. Moreover, the mechanism of energy transfer from Gd^{3+} to Dy^{3+} is investigated. The band gaps of un-doped and Dy^{3+} doped $Ca_9Gd(PO_4)_7$ were calculated to be 3.88 and 3.87 eV, respectively. The internal quantum efficiency and external quantum efficiency of as-obtained phosphors under 350 nm excitation are determined to be 19.9 and 9.2%, respectively. The PL intensity at 100, 150, and 200 °C is about 85, 76, and 59% of the initial intensity at room temperature, respectively. Our studies indicate that our phosphors have potential applications in solid-state luminescence.

Acknowledgements This work is financially supported by the Science and Technology Program of Guangzhou, China (201707010324, 201607010345), Key Platforms and Research Projects of Department of Education of Guangdong Province (2016KTSCX031, 2016KTSCX034), National Natural Science Foundation of China (11674310, 11704078, 61704034), Pearl River S&T Nova Program of Guangzhou (201710010143) and Innovation and Entrepreneurship Training Programs (201611845030, 201611845141 and yj201611845348) for Chinese College Students.

References

1. E.F. Schubert, J.K. kim, Science. **308**, 1274 (2005)
2. M.M. Shang, C.X. Li, J. Lin, Chem. Soc. Rev. **43**, 1372 (2014)
3. S. Ye, F. Xiao, Y.X. Pan, Y.Y. Ma, Q.Y. Zhang, Mater. Sci. Eng. **71**, 1 (2010)
4. X. Shen, D.F. Zhang, X.W. Fan, G.S. Hu, X.B. Bian, L. Yang, J. Mater. Sci. Mater. El. **27**, 976 (2016)
5. H.L. Shi, C. Zhu, J.Q. Huang, J. Chen, D.C. Chen, W.C. Wang, F.Y. Wang, Y.G. Cao, X.Y. Yuan, Opt. Mater. Express. **4**, 649 (2014)
6. C.H. Huang, P.J. Wu, J.F. Lee, T.M. Chen, J. Mater. Chem. **21**, 10489 (2011)
7. J.S. Kim, P.E. Jeon, Y.H. Park, J.C. Choi, H.L. Park, J. Electochem. Soc. **152**, H29 (2005)
8. Y. Liu, G.X. Liu, J.X. Wang, X.T. Dong, W.S. Yu, Inorg. Chem. **53**, 11457 (2014)
9. Y.M. Deng, S.P. Yi, J. Huang, J.Q. Xian, W.R. Zhao, Mater. Res. Bull. **57**, 85 (2014)
10. Z.W. Zhang, A.J. Song, X.H. Shen, Q. Lian, X.F. Zheng, Mater. Chem. Phys. **151**, 345 (2015)
11. M. Yu, J. Lin, Z. Wang, J. Fu, S. Wang, H.J. Zhang, Y.C. Han, Chem. Mater. **14**, 2224 (2002)
12. K.N. Shinde, I.M. Nagpure, S.J. Dhoble, S.V. Godbole, M.K. Bhide, Indian J. Phys. **83**, 503 (2009)
13. T. Selvalakshmi, S. Sellaiyan, A. Uedono, A.C. Bose, RSC Adv. **65**, 34257 (2014)
14. N. Guo, Y.J. Huang, H.P. You, M. Yang, Y.H. Song, K. Liu, Y.H. Zheng, Inorg. Chem. **49**, 10907 (2010)
15. W.Y. Geng, G. Zhu, Y.R. Shi, Y.H. Wang, J. Lumin. **155**, 205 (2014)
16. Z.Z. Zhu, G.S. Fu, Y. Yang, Z.P. Yang, P.L. Li, J. Mater. Chem. **51**, 6944 (2016)
17. Y.W. Seo, S.H. Park, S.H. Chang, J.H. Jeong, K.H. Kim, J.S. Bae, Ceram. Int. **43**, 8497 (2017)
18. R.D. Shannon, Acta Crysta. **32**, 751 (1976)
19. S.K. Sharma, S. Som, R. Jain, A.K. Kunti, J. Lumin. **159**, 317 (2015)
20. J. Tauc, A. Menth, J. Non-Cryst. Solids. **8–10**, 569 (1972)
21. Z.W. Zhang, Y.J. Ren, L. Liu, J.P. Zhang, Y.S. Peng, Luminescence. **30**, 1190 (2015)
22. X.L. Dong, J.H. Zhang, X. Zhang, Z.D. Hao, S.Z. Lv, Ceramics Int. **40**, 5421 (2014)
23. Z.H. Liang, Z.F. Mu, Q. Wang, D.Y. Zhu, F.G. Wu, Appl. Phys. A. **123**, 612 (2017)
24. H. Yu, D.G. Deng, Y.Q. Li, S.Q. Xu, Y.Y. Li, C.P. Yu, Y.Y. Ding, H.W. Lu, H.Y. Yin, Q.L. Nie, J. Lumin. **143**, 132 (2013)
25. Z.W. Zhang, A.J. Song, Y. Yue, H. Zhong, X.Y. Zhang, M.Z. Ma, R.P. Liu, J. Alloys Compd. **650**, 410 (2015)
26. M. Trevisani, K.V. Ivanovskikh, F. Piccinelli, A. Speghini, M. Bettinelli, J. Phys.: Condens. Matter. **24**, 385502 (2012)
27. X.M. Zhang, F.G. Meng, W.L. Li, S.I. Kim, Y.M. Yu, H.J. Seo, J. Alloys Compd. **578**, 72 (2013)
28. J. Holsa, R.J. Lamminmaki, M. Lastusaari, P. Porcher, J. Alloys Compd. **323–324**, 811 (2001)
29. G. Blasse, Philips Res. Rep. **24**, 131 (1969)
30. G. Blasse, J. Solid State Chem. **62**, 207 (1986)
31. Y.H. Jin, Y.H. Hu, H.Y. Wu, H. Duan, L. Chen, Y.R. Fu, G.F. Ju, Z.F. Mu, M. He, Chem. Eng. J. **288**, 596 (2017)
32. L.G.V. Uitert, J. Electrochem. Soc. **114**, 1048 (1976)
33. R. Pang, C.Y. Li, L.L. Shi, Q. Su, J. Phys. Chem. Solids. **70**, 303 (2009)
34. Q. Su, Z.W. Pei, L.S. Chi, H.J. Zhang, Z.Y. Zhang, F. Zou, J. Alloys Compd. **192**, 25 (1993)
35. Q. Su, H.B. Liang, C.Y. Li, H. He, Y.H. Lu, J. Li, Y. Tao, J. Lumin. **122–123**, 927 (2007)
36. B.C. Jamalaiah, M. Jo, Z.H. Jiang, J.J. Shim, S.I. Kim, W.Y. Chung, H.J. Seo, Opt. Mater. **36**, 1688 (2014)
37. M.H. Tong, Y.J. Liang, G.G. Li, Z.G. Xia, M.F. Zhang, F. Yang, Q. Wang, Opt. Mater. **36**, 1566 (2014)